Online Appendix

Air Service Hub Network Design for Express Delivery Operations

Kaixiang Tang, Ling Zhu, Lingxiao Wu, Jean-François Cordeau, Yixiao Huang

Appendix A: Mathematical Proofs

This section presents proofs of the propositions and theorems in the main text.

A.1. Proof of Proposition 1

Proof. For any given $(\bar{\boldsymbol{x}}, \bar{\boldsymbol{y}}) \in \mathcal{X}$, set $g_{ikm} = \bar{x}_{ik} \sum_{j \in \mathcal{N}} w_{ij} \bar{x}_{jm}$ for all $i \in \mathcal{N}$ and $k, m \in \mathcal{H}$ with $k \neq m$. Because each node is allocated to exactly one hub, this solution satisfies constraints (31) and (32). Setting $\boldsymbol{\theta} = \mathbf{0}$ and $\phi_{km} = \sum_{i \in \mathcal{N}} g_{ikm}$ then satisfies all the remaining BSP constraints. Hence, the BSP is feasible. Moreover, its objective value is bounded below by zero, and the constructed solution has a finite objective value. The BSP therefore has a finite optimal value, so strong duality implies that the BDSP is feasible and has the same finite optimal value. □

A.2. Proof of Proposition 2

Proof. Upon convergence of CG, the dual values $(\boldsymbol{\pi}^*, \boldsymbol{\lambda}^*, \boldsymbol{\alpha}^*, \boldsymbol{\beta}^*, \boldsymbol{\rho}^*)$ satisfy constraints (40)–(44), while the construction in (51) ensures that $\boldsymbol{\chi}^*$ satisfies constraints (45). It remains to verify constraints (39). For every $r \in \mathcal{R}'$, all hubs visited by r belong to $\mathcal{H}'$, and hence $\chi_k^{v*} = 0$ for every $k \in \mathcal{H}(r)$. Upon convergence of CG, no route in $\mathcal{R}'$ has a negative reduced cost; therefore, constraints (39) are satisfied for every $r \in \mathcal{R}'$. Consider any $r \in \mathcal{R} \setminus \mathcal{R}'$ and select $k_0 \in \mathcal{H}(r) \setminus \mathcal{H}'$. By the definition of the route cost and the nonnegativity of μ_{km}^v, we have $\bar{c}_r^v \geq \kappa_v$. Since $o_r, d_r \in \mathcal{H}$, we have $-\beta_{o_r}^{v*} + \beta_{d_r}^{v*} \geq -\max_{k \in \mathcal{H}} \beta_k^{v*} + \min_{k \in \mathcal{H}} \beta_k^{v*}$. Constraints (41) give $\rho_{km}^* \geq -\gamma$, while the definition of a feasible route gives $\sum_{(k,m) \in \mathcal{A}_H} B_{rkm} \leq L$. Therefore,

$$\bar{c}_r^v - \alpha_v^* - \beta_{o_r}^{v*} + \beta_{d_r}^{v*} + \sum_{(k,m) \in \mathcal{A}_H} B_{rkm} U_v \rho_{km}^* \geq \kappa_v - \alpha_v^* - \max_{k \in \mathcal{H}} \beta_k^{v*} + \min_{k \in \mathcal{H}} \beta_k^{v*} - L U_v \gamma \geq \chi_{k_0}^{v*}, \tag{A.1}$$

where the last inequality follows from (51). Since $\boldsymbol{\chi}^* \leq \mathbf{0}$, $-\sum_{k \in \mathcal{H}(r)} \chi_k^{v*} \geq -\chi_{k_0}^{v*}$. Together with the constraints already satisfied for $r \in \mathcal{R}'$, this shows that $(\boldsymbol{\pi}^*, \boldsymbol{\lambda}^*, \boldsymbol{\alpha}^*, \boldsymbol{\beta}^*, \boldsymbol{\rho}^*, \boldsymbol{\chi}^*)$ satisfies constraints (39) for every $r \in \mathcal{R}$ and is feasible for the BDSP. Constraints (36) force $\theta_r^v = 0$ for $r \in \mathcal{R} \setminus \mathcal{R}'$, so replacing $\mathcal{R}$ with $\mathcal{R}'$ in the BSP does not change its optimal value. Moreover, $\chi_k^{v*} \bar{y}_k = 0$ for every $v \in \mathcal{V}$ and $k \in \mathcal{H}$. Therefore, the completed dual solution has the same objective value as the RMP dual solution obtained at convergence of CG. By strong duality, this value equals the optimal BSP value; hence, the associated cut is tight at $(\bar{\boldsymbol{x}}, \bar{\boldsymbol{y}})$. Since the BDSP constraints are independent of $(\boldsymbol{x}, \boldsymbol{y})$, this solution is dual feasible for every $(\boldsymbol{x}, \boldsymbol{y}) \in \mathcal{X}$, and weak duality establishes the validity of the associated Benders optimality cut throughout $\mathcal{X}$. □

A.3. Proof of Lemma 1

Proof. Suppose, for contradiction, that Λ_E^v is integral for every aircraft type $v \in \mathcal{V}$, sequence length $\iota \in \{2, \ldots, L\}$, and sequence $E \in \mathcal{S}_\iota$. Since $\boldsymbol{\theta}^*$ is fractional, select a fractional component $\theta_{r_1}^{v_1 *}$ such that route r_1 has the maximum number L' of flight legs among all routes associated with fractional components. We first show that $L' \geq 2$. If $L' = 1$, let e be the only flight leg of r_1. Any other route containing e either has more than one flight leg and thus has an

integral route variable by the choice of r_1, or is identical to r_1. It follows that $\Gamma_e^{v_1}$ equals the fractional value $\theta_{r_1}^{v_1*}$ plus integral contributions and is therefore fractional, contradicting the integrality of $\boldsymbol{\Gamma}$. Hence, $2 \le L' \le L$. Let $E \in \mathcal{S}_{L'}$ be the complete sequence of flight legs in r_1. Since distinct routes correspond to distinct flight-leg sequences, every other route containing E has more than L' flight legs and thus has an integral route variable by the choice of r_1. Therefore, $\Lambda_E^{v_1} = \theta_{r_1}^{v_1*} + \sum_{r \in \mathcal{R}\setminus\{r_1\}:K_{r,E}=1} \theta_r^{v_1*}$ is fractional, contradicting the assumed integrality of Λ_E^v for all $v \in \mathcal{V}$, $\iota \in \{2,\dots,L\}$, and $E \in \mathcal{S}_\iota$. Therefore, there exists a fractional Λ_E^v for some $v \in \mathcal{V}$, $\iota \in \{2,\dots,L\}$, and $E \in \mathcal{S}_\iota$. □

A.4. Proof of Theorem 1

Proof. At each node of the branch-and-bound tree, the algorithm solves the relaxed model $\overline{\text{M2}}$ to optimality using BD. The resulting objective value provides a valid local lower bound because $\overline{\text{M2}}$ is a relaxation of M2 at the current node. The global lower bound is maintained as the minimum of the local lower bounds over all active nodes. During the branching phase, Lemma 1 ensures that, for any fractional solution $\boldsymbol{\theta}^*$, a fractional auxiliary sequence variable Λ_E^v can always be identified to partition the current solution. Therefore, the proposed branching scheme is complete and enforces the integrality of $\boldsymbol{\theta}$. Any feasible integer solution found during the search updates the global upper bound. Since the discrete solution space is finite, the branch-and-bound tree is finite. Together with the exact local lower bounds obtained from BD and the progressively updated global upper bound, the standard branch-and-bound fathoming rules guarantee convergence to the global optimal integer solution of M2. □

A.5. Proof of Proposition 3

Proof. Given any feasible solution $(\bar{\boldsymbol{x}}, \bar{\boldsymbol{y}}) \in \mathcal{X}$, let $(\boldsymbol{g}^*, \boldsymbol{\theta}^*, \boldsymbol{\phi}^*)$ be an optimal BSP solution with objective value Z_S^*. For each $(k,m) \in \mathcal{A}_H$, define $a_{km} := \min_{v \in \mathcal{V}}\{(\mu_{km}^v + \kappa_v/L)/U_v\}$. Let $Z_{\text{LB}}(\bar{\boldsymbol{x}}, \bar{\boldsymbol{y}})$ denote the minimum value of the right-hand side of (53) over $\boldsymbol{g}$ satisfying constraints (7) and (8) for the given $(\bar{\boldsymbol{x}}, \bar{\boldsymbol{y}})$.

Because $\boldsymbol{g}^*$ satisfies constraints (7) and (8), it is feasible in the definition of $Z_{\text{LB}}(\bar{\boldsymbol{x}}, \bar{\boldsymbol{y}})$. By the capacity constraints (35),

$$Z_{\text{LB}}(\bar{\boldsymbol{x}}, \bar{\boldsymbol{y}}) \le \sum_{(k,m)\in\mathcal{A}_H} a_{km} \sum_{i \in \mathcal{N}} g_{ikm}^* \le \sum_{(k,m)\in\mathcal{A}_H} a_{km} \left(\sum_{v\in\mathcal{V}} \sum_{r\in\mathcal{R}} B_{rkm} U_v \theta_r^{v*} + \phi_{km}^* \right). \tag{A.2}$$

By the definition of a_{km}, we have $a_{km} U_v \le \mu_{km}^v + \kappa_v/L$ for every $v \in \mathcal{V}$. Moreover, by the condition stated before (53), $a_{km} \le \gamma$. Since $\boldsymbol{\theta}^*$ and $\boldsymbol{\phi}^*$ are nonnegative, it follows that

$$\sum_{(k,m)\in\mathcal{A}_H} a_{km} \left(\sum_{v\in\mathcal{V}} \sum_{r\in\mathcal{R}} B_{rkm} U_v \theta_r^{v*} + \phi_{km}^* \right) \le \sum_{v\in\mathcal{V}} \sum_{r\in\mathcal{R}} \sum_{(k,m)\in\mathcal{A}_H} \left(\mu_{km}^v + \frac{\kappa_v}{L} \right) B_{rkm} \theta_r^{v*} + \sum_{(k,m)\in\mathcal{A}_H} \gamma \phi_{km}^*. \tag{A.3}$$

Each route $r \in \mathcal{R}$ contains at most L flight legs, so $\sum_{(k,m)\in\mathcal{A}_H} B_{rkm} \le L$. Therefore,

$$\begin{aligned} &\sum_{v\in\mathcal{V}} \sum_{r\in\mathcal{R}} \sum_{(k,m)\in\mathcal{A}_H} \left(\mu_{km}^v + \frac{\kappa_v}{L} \right) B_{rkm} \theta_r^{v*} + \sum_{(k,m)\in\mathcal{A}_H} \gamma \phi_{km}^* \\ &\qquad \le \sum_{v\in\mathcal{V}} \sum_{r\in\mathcal{R}} \left(\kappa_v + \sum_{(k,m)\in\mathcal{A}_H} B_{rkm} \mu_{km}^v \right) \theta_r^{v*} + \sum_{(k,m)\in\mathcal{A}_H} \gamma \phi_{km}^* = Z_S^*. \end{aligned} \tag{A.4}$$

Combining inequalities (A.2)–(A.4) gives $Z_{\text{LB}}(\bar{\boldsymbol{x}}, \bar{\boldsymbol{y}}) \le Z_S^*$. Thus, $Z_{\text{LB}}(\bar{\boldsymbol{x}}, \bar{\boldsymbol{y}})$ is a valid lower bound on the optimal BSP value. Constraints (7), (8), and (53) provide an extended formulation of $\eta \ge Z_{\text{LB}}(\boldsymbol{x}, \boldsymbol{y})$ and are therefore valid for the BMP. □

A.6. Proof of Proposition 4

Proof. As described in Theorem 1, at each node of the branch-and-bound tree, we solve $\overline{\text{M2}}$. Any integer feasible solution to $\overline{\text{M2}}$ is also a feasible solution to M2. According to Benders (1962), the solution obtained in any iteration of Benders decomposition is feasible for $\overline{\text{M2}}$. Therefore, any integer solution $\boldsymbol{\theta}^*$ encountered in any iteration of the algorithm yields a feasible solution to M2. □

Appendix B: Notation for the ASHNDP Formulations and Solution Approach

The principal sets and parameters used in the ASHNDP formulations and solution approach are summarized in Table B.1. The corresponding decision variables are listed in Table B.2.

Table B.1 Sets and Parameters Used in the ASHNDP Formulations and Solution Approach

Notation	Description
$\mathcal{N}$	set of nodes
$\mathcal{H}$	set of potential hub nodes
$\mathcal{A}$	set of arcs
$\mathcal{A}_{\mathcal{H}}$	set of arcs between potential hub nodes
$\mathcal{Q}$	set of cargo aircraft
$\mathcal{V}$	set of cargo aircraft types
$\mathcal{Q}_v$	set of type $v \in \mathcal{V}$ cargo aircraft
$\mathcal{R}$	set of feasible cargo aircraft routes
T	length of the planning horizon
L	maximum number of flights a cargo aircraft can operate within the planning horizon T
$[L]$	set of flight-leg indices for a cargo aircraft
p	number of hubs chosen in the network
f_k	daily fixed cost of opening hub $k \in \mathcal{H}$
S_k	handling capacity of hub $k \in \mathcal{H}$
ω_k	turnaround time at hub $k \in \mathcal{H}$
τ_{km}	travel time of cargo aircraft flying from hub $k \in \mathcal{H}$ to hub $m \in \mathcal{H}$
U_q, U_v	capacities of cargo aircraft $q \in \mathcal{Q}$ and a cargo aircraft of type $v \in \mathcal{V}$, respectively
c_{ik}	unit ground transportation cost from spoke $i \in \mathcal{N}$ to hub $k \in \mathcal{H}$
c_{ki}	unit ground transportation cost from hub $k \in \mathcal{H}$ to spoke $i \in \mathcal{N}$
κ_q, κ_v	daily fixed operating costs of cargo aircraft $q \in \mathcal{Q}$ and a cargo aircraft of type $v \in \mathcal{V}$, respectively
μ^q_{km}, μ^v_{km}	transport costs of traversing hub arc $(k,m) \in \mathcal{A}_{\mathcal{H}}$ by cargo aircraft $q \in \mathcal{Q}$ and a cargo aircraft of type $v \in \mathcal{V}$, respectively
o_r, d_r	origin and destination hubs of route $r \in \mathcal{R}$, respectively
B_{rkm}	number of times route $r \in \mathcal{R}$ traverses hub arc $(k,m) \in \mathcal{A}_{\mathcal{H}}$
$\bar{c}^v_r$	operating cost of assigning a cargo aircraft of type $v \in \mathcal{V}$ to route $r \in \mathcal{R}$
γ	unit weight penalty cost of delayed cargo
w_{ij}	daily weight of demand originating from node $i \in \mathcal{N}$ and destined to node $j \in \mathcal{N}$
$O_i = \sum_{j \in \mathcal{N}} w_{ij}$	total flow originating at node $i \in \mathcal{N}$
$D_j = \sum_{i \in \mathcal{N}} w_{ij}$	total flow destined to node $j \in \mathcal{N}$

Appendix C: Additional Details of the BD-B&B Approach

In this section, we provide additional details of the BD-B&B approach.

Table B.2 Decision Variables Used in the ASHNDP Formulations and Solution Approach

Notation	Description
x_{ik}	binary variable, which takes value 1 if and only if node $i \in \mathcal{N}$ is allocated to hub node $k \in \mathcal{H}$
y_k	binary variable, which takes value 1 if and only if potential hub location $k \in \mathcal{H}$ is selected as a hub node
g_{ikm}	continuous variable, which represents the amount of flow originating at node $i \in \mathcal{N}$ that is routed via hub $k \in \mathcal{H}$ and hub $m \in \mathcal{H}$
ϕ_{km}	continuous variable, which represents the amount of flow that cannot be shipped from hub $k \in \mathcal{H}$ to hub $m \in \mathcal{H}$ within the planning horizon
δ_q	binary variable, which takes value 1 if and only if cargo aircraft $q \in \mathcal{Q}$ is purchased by the carrier
z^{ql}_{km}	binary variable, which takes value 1 if and only if cargo aircraft $q \in \mathcal{Q}$ traverses hub arc $(k,m) \in \mathcal{A}_{\mathcal{H}}$ as its l-th flight leg, where $l \in [L]$
θ^v_r	integer variable, which represents the number of type-v cargo aircraft assigned to route $r \in \mathcal{R}$
η	continuous surrogate variable in the BMP, which represents the objective function value of the BSP

C.1. The Benders Decomposition Algorithm

Let LB' and UB' denote the lower bound and upper bound of Benders decomposition. The details of the Benders decomposition algorithm are presented in Algorithm C.1. Let $\widehat{\Delta} \subseteq \Delta$ denote the set of dual solutions whose corresponding Benders optimality cuts have been added to the restricted BMP.

Algorithm C.1 Benders Decomposition Algorithm

Input: $\overline{\text{M2}}$ at a node in the branch-and-bound tree.
Output: Optimal solution $(\boldsymbol{x}^*, \boldsymbol{y}^*, \boldsymbol{g}^*, \boldsymbol{\theta}^*, \boldsymbol{\phi}^*)$ and optimal objective value Z_M^* of $\overline{\text{M2}}$.
$LB' \leftarrow -\infty$, $UB' \leftarrow +\infty$, $\text{gap} \leftarrow +\infty$, $\widehat{\Delta} \leftarrow \emptyset$. Set tolerance $\epsilon = 0.1\%$.
while $\text{gap} > \epsilon$ **do**
    Solve the restricted BMP containing the Benders optimality cuts associated with the dual solutions in $\widehat{\Delta}$ to obtain optimal solution $(\bar{\boldsymbol{x}}, \bar{\boldsymbol{y}}, \bar{\eta})$ and objective value $\bar{Z}_M$.
    if $\bar{Z}_M > LB'$ **then**
        $LB' \leftarrow \bar{Z}_M$.
    end if
    Solve the BSP by column generation (see Section 4.4) to obtain optimal solution $(\bar{\boldsymbol{g}}, \bar{\boldsymbol{\theta}}, \bar{\boldsymbol{\phi}})$, dual values $(\bar{\boldsymbol{\pi}}, \bar{\boldsymbol{\lambda}}, \bar{\boldsymbol{\alpha}}, \bar{\boldsymbol{\beta}}, \bar{\boldsymbol{\rho}}, \bar{\boldsymbol{\chi}})$, and objective value $\bar{Z}_S$.
    if $\bar{Z}_M - \bar{\eta} + \bar{Z}_S < UB'$ **then**
        $UB' \leftarrow \bar{Z}_M - \bar{\eta} + \bar{Z}_S$; $(\boldsymbol{x}^*, \boldsymbol{y}^*, \boldsymbol{g}^*, \boldsymbol{\theta}^*, \boldsymbol{\phi}^*) \leftarrow (\bar{\boldsymbol{x}}, \bar{\boldsymbol{y}}, \bar{\boldsymbol{g}}, \bar{\boldsymbol{\theta}}, \bar{\boldsymbol{\phi}})$.
    end if
    Update $\widehat{\Delta} \leftarrow \widehat{\Delta} \cup \{(\bar{\boldsymbol{\pi}}, \bar{\boldsymbol{\lambda}}, \bar{\boldsymbol{\alpha}}, \bar{\boldsymbol{\beta}}, \bar{\boldsymbol{\rho}}, \bar{\boldsymbol{\chi}})\}$; $\text{gap} \leftarrow (UB' - LB')/UB'$.
end while
$Z_M^* = UB'$.
return $(\boldsymbol{x}^*, \boldsymbol{y}^*, \boldsymbol{g}^*, \boldsymbol{\theta}^*, \boldsymbol{\phi}^*)$ and Z_M^*.

C.2. The Labeling Algorithm for Solving the PP

This section describes the labeling algorithm for solving the pricing problems that arise when using CG to solve the BSP. Algorithm C.2 presents the pseudocode of this procedure.

Algorithm C.2 Labeling Algorithm for Graph $\bar{G}_v$

Input: $\bar{G}_v$, T.
Output: Shortest path r^*, best cost $\tilde{c}^*$.
Initialize label set $\mathcal{L}_n = \emptyset$ for each node $n \in \bar{\mathcal{H}}'$ and set $\tilde{c}^* \leftarrow +\infty$.
Create initial label $\ell_O = (O, (O), 0, 0, 0)$. Add ℓ_O to label set $\mathcal{L}_O$ and push ℓ_O into queue Q.
while $Q \neq \emptyset$ **do**
    Select a label ℓ from Q and update $Q \leftarrow Q \setminus \{\ell\}$.
    if $n(\ell) = D$ **and** $t(\ell) \leq T$ **and** $\tilde{c}(\ell) < \tilde{c}^*$ **then**
        $r^* \leftarrow \Psi(\ell)$. $\tilde{c}^* \leftarrow \tilde{c}(\ell)$.
    end if
    for each $(n(\ell), j) \in \bar{\mathcal{A}}'_{\mathcal{H}}$ **do**
        if $t(\ell) + t_{n(\ell),j} \leq T$ **then**
            $n(\ell') \leftarrow j$; append j to $\Psi(\ell)$ to obtain $\Psi(\ell')$; $h(\ell') \leftarrow h(\ell) + 1$ if $(n(\ell), j) \in \mathcal{A}'_{\mathcal{H}}$, and $h(\ell') \leftarrow h(\ell)$ otherwise;
            $\tilde{c}(\ell') \leftarrow \tilde{c}(\ell) + \tilde{\mu}^v_{n(\ell),j}$, $t(\ell') \leftarrow t(\ell) + t_{n(\ell),j}$.
            $\ell' \leftarrow (n(\ell'), \Psi(\ell'), h(\ell'), \tilde{c}(\ell'), t(\ell'))$. $\mathcal{L}_j \leftarrow \mathcal{L}_j \cup \{\ell'\}$. $Q \leftarrow Q \cup \{\ell'\}$.
            Remove dominated labels in $\mathcal{L}_j$.
        end if
    end for
end while
return r^* and $\tilde{c}^*$.

In this algorithm, a partial path from the dummy source node O to node n is encoded as a label $\ell = (n(\ell), \Psi(\ell), h(\ell), \tilde{c}(\ell), t(\ell))$, where $n(\ell)$ is its last visited node, $\Psi(\ell)$ is the sequence of nodes in the partial path, $h(\ell)$ is its number of flight legs, and $\tilde{c}(\ell)$ and $t(\ell)$ are its accumulated arc cost and travel time, respectively.

In the forward extension process, the label ℓ can extend along arc $(n(\ell), j) \in \bar{\mathcal{A}}'_{\mathcal{H}}$. The node sequence $\Psi(\ell')$ is obtained by appending j to $\Psi(\ell)$. Then a new label ℓ' is generated and the values of attributes are set as follows:

$$n(\ell') = j, \qquad h(\ell') = \begin{cases} h(\ell)+1, & (n(\ell), j) \in \mathcal{A}'_{\mathcal{H}}, \\ h(\ell), & \text{otherwise}, \end{cases}$$
$$\tilde{c}(\ell') = \tilde{c}(\ell) + \tilde{\mu}^{v}_{n(\ell),j}, \quad t(\ell') = t(\ell) + t_{n(\ell),j}.$$

Then, we verify if this label ℓ' is feasible with respect to the time limit. If its accumulated travel time $t(\ell')$ exceeds T, label ℓ' is deemed infeasible and discarded. Crucially, the strictly increasing accumulated travel time, bounded by the finite length of planning horizon T, guarantees finite termination without subtour elimination constraints. Besides, to reduce the number of labels, a dominance rule is embedded in the algorithm. We say that a label ℓ_1 dominates a label ℓ_2 if they share the same last visited node (i.e., $n(\ell_1) = n(\ell_2)$) and the same number of flight legs (i.e., $h(\ell_1) = h(\ell_2)$), ℓ_1 has a lower or equal accumulated cost than ℓ_2 (i.e., $\tilde{c}(\ell_1) \leq \tilde{c}(\ell_2)$), and ℓ_1 also has a smaller or equal accumulated travel time than ℓ_2 (i.e., $t(\ell_1) \leq t(\ell_2)$). The dominated labels are then removed from the algorithm.

C.3. The Column Generation Algorithm

The detailed procedure of the overall CG algorithm described in Section 4.4 is presented in Algorithm C.3.

Algorithm C.3 Column Generation Algorithm

Input: $(\boldsymbol{x}^*, \boldsymbol{y}^*)$ from the BMP.
Output: Optimal primal BSP solution $(\boldsymbol{g}^*, \boldsymbol{\theta}^*, \boldsymbol{\phi}^*)$; BSP objective value Z^*_S; BDSP dual solution $(\boldsymbol{\pi}^*, \boldsymbol{\lambda}^*, \boldsymbol{\alpha}^*, \boldsymbol{\beta}^*, \boldsymbol{\rho}^*, \boldsymbol{\chi}^*)$.
Initialize reduced cost $\tilde{c}_0 = -0.001$ and the initial column sets of cargo aircraft routes $\mathcal{R}'_s$ for the RMP.
Set the initial values of dual variables $(\boldsymbol{\pi}^*, \boldsymbol{\lambda}^*, \boldsymbol{\alpha}^*, \boldsymbol{\beta}^*, \boldsymbol{\rho}^*)$ all to zero and optimal objective value $Z^*_S \leftarrow -\infty$.
while $\tilde{c}_0 < 0$ **do**
    Solve the RMP to update optimal solution $(\boldsymbol{g}^*, \boldsymbol{\theta}^*, \boldsymbol{\phi}^*)$, update values of dual variables $(\boldsymbol{\pi}^*, \boldsymbol{\lambda}^*, \boldsymbol{\alpha}^*, \boldsymbol{\beta}^*, \boldsymbol{\rho}^*)$, and optimal objective value Z^*_S.
    for each cargo aircraft type $v \in \mathcal{V}$ **do**
        Generate $\bar{G}_v = (\bar{\mathcal{H}}', \bar{\mathcal{A}}'_{\mathcal{H}})$ using $(\boldsymbol{x}^*, \boldsymbol{y}^*)$ and the current RMP dual solution.
        Apply Algorithm C.2 to obtain the shortest route r^*_v with path cost $\tilde{c}^*_v$.
        Calculate $\tilde{c}^v_{r^*_v} = \tilde{c}^*_v + \kappa_v - \alpha_v$.
    end for
    Get the lowest reduced cost $\tilde{c}_{\min} = \min_{v \in \mathcal{V}} \tilde{c}^v_{r^*_v}$.
    Add each cargo aircraft route r^*_v with $\tilde{c}^v_{r^*_v} < 0$ to set $\mathcal{R}'_s$, and put set $\mathcal{R}'_s$ into the RMP.
    $\tilde{c}_0 \leftarrow \tilde{c}_{\min}$.
end while
Construct $\boldsymbol{\chi}^*$ according to (51).
return $(\boldsymbol{g}^*, \boldsymbol{\theta}^*, \boldsymbol{\phi}^*)$, Z^*_S, and $(\boldsymbol{\pi}^*, \boldsymbol{\lambda}^*, \boldsymbol{\alpha}^*, \boldsymbol{\beta}^*, \boldsymbol{\rho}^*, \boldsymbol{\chi}^*)$.

C.4. Treatment of Branching Constraints in the BSP

Adding the branching constraints into the BSP affects its structure in the following ways.

C.4.1. Adjustments to the Pricing Problem. The dual variables that come from the branching constraints should be considered in the pricing problem of CG. In particular, for the first branching rule, if $\lfloor \Xi_{\bar{k}\bar{m}} \rfloor$ is set to be zero, the arc $(\bar{k}, \bar{m})$ is removed from all the state-space graphs to avoid the generation of aircraft routes passing through this arc. For the second branching rule, if $\lfloor \Gamma^{\bar{v}}_{\bar{e}} \rfloor$ is zero, where $\bar{e} = (\bar{k}, \bar{m}, \bar{l})$, a label cannot be extended from $\bar{k}$ to $\bar{m}$ when generating its $\bar{l}$-th flight leg in state-space graph $\bar{G}_{\bar{v}}$. Similarly, for the third branching rule, if $\lfloor \Lambda^{\bar{v}}_{\bar{E}} \rfloor$ is zero, any extension that completes sequence $\bar{E}$ is discarded in $\bar{G}_{\bar{v}}$. For the other branching cases, they are handled by integrating the corresponding dual values into the associated costs in the pricing problem.

C.4.2. Adjustments to the Dominance Rule. As discussed by Desaulniers et al. (2020), branching decisions may affect the validity of dominance rules in a labeling algorithm. In our approach, the dominance rule must be modified when constraints generated by the third (follow-on) branching rule are active. At a given branch-and-bound node, let $\mathcal{B}^v$ be the set of flight-leg sequences specified by the active follow-on branching constraints for aircraft type $v \in \mathcal{V}$. For each $E \in \mathcal{B}^v$, let ι_E denote its number of flight legs and let $E = (e_1, \ldots, e_{\iota_E})$, where $e_\varpi = (k_\varpi, m_\varpi, l_\varpi)$ for $\varpi = 1, \ldots, \iota_E$. For a label ℓ, let $F_l(\ell)$ denote the l-th flight leg of its partial route. For each $E \in \mathcal{B}^v$ with $h(\ell) < l_{\iota_E}$, define the binary label component $s_E(\ell)$ as follows. If $h(\ell) < l_1$, set $s_E(\ell) = 1$. If $l_1 \le h(\ell) < l_{\iota_E}$, set

$$s_E(\ell) := \begin{cases} 1, & F_{l_\varpi}(\ell) = e_\varpi \quad \forall \varpi \in \{1, \ldots, \iota_E\} \text{ with } l_\varpi \le h(\ell), \\ 0, & \text{otherwise.} \end{cases}$$

Hence, $s_E(\ell) = 1$ precisely when the partial route can still contain E after further extensions, based on the flight legs already generated. Let $\mathcal{U}^v(h) = \{E \in \mathcal{B}^v : h < l_{\iota_E}\}$ and $\boldsymbol{s}(\ell) = (s_E(\ell))_{E \in \mathcal{U}^v(h(\ell))}$. We add $\boldsymbol{s}(\ell)$ to the label and retain the original dominance conditions with the additional requirement $\boldsymbol{s}(\ell_1) = \boldsymbol{s}(\ell_2)$.

PROPOSITION C.1. *The revised dominance rule is valid when constraints generated by the third branching rule are active.*

Proof. Let $\widehat{E}$ be any ordered sequence of subsequent flight legs that extends the partial route represented by ℓ_2 to a feasible complete route, and extend the partial route represented by ℓ_1 by the same sequence. Since $n(\ell_1) = n(\ell_2)$ and $h(\ell_1) = h(\ell_2)$, the flight legs in $\widehat{E}$ traverse the same hub arcs at the same ordinal numbers in both extensions. The first branching rule depends only on the hub arc, while the second depends only on the aircraft type, hub arc, and ordinal number; hence, the two extensions are subject to the same restrictions under these rules and receive the same corresponding dual terms. Moreover, $t(\ell_1) \le t(\ell_2)$ ensures that the extension from ℓ_1 satisfies the time limit of the planning horizon whenever that from ℓ_2 does. It remains to consider the third (follow-on) branching rule. For sequences whose final ordinal numbers have already been reached, infeasible labels have been discarded and any applicable dual terms are already included in the accumulated reduced costs. It therefore suffices to consider $E \in \mathcal{U}^v(h(\ell_1))$. For each such E, equality $\boldsymbol{s}(\ell_1) = \boldsymbol{s}(\ell_2)$ ensures that the complete routes obtained by appending $\widehat{E}$ either both contain E or neither does. If the corresponding branching constraint is $\sum_{r \in \mathcal{R}} K_{r,E} \theta_r^v \le 0$, the nonnegativity of $\boldsymbol{\theta}$ excludes every route containing E; hence, the extension is permitted for both labels or for neither. Under every other active follow-on branching constraint associated with E, the corresponding dual term affects the reduced costs of the two routes equally. Thus, $\widehat{E}$ yields a feasible complete route from ℓ_1 whenever it does from ℓ_2, and the two extensions have identical reduced-cost increments. Together with $\widetilde{c}(\ell_1) \le \widetilde{c}(\ell_2)$, this implies that the route generated from ℓ_1 has no greater reduced cost, so ℓ_2 can be safely discarded. □

If $\mathcal{B}^v = \emptyset$, the revised rule reduces to the original rule. The added label vector contains one binary component per unfinished active sequence and is used only when the third branching rule is active; its effect on computational performance is therefore expected to be limited.

C.4.3. Adjustments to the Benders Optimality Cuts. The dual variables that come from the branching constraints should also be incorporated into optimality cuts (48). Specifically, let Υ denote the index set of all active branching constraints imposed on the BSP at the current node. For each active branching constraint $\psi \in \Upsilon$, let u_ψ denote its constant right-hand side value (which takes the form of $\lfloor \Xi_{\bar{k}\bar{m}} \rfloor$, $\lceil \Xi_{\bar{k}\bar{m}} \rceil$, $\lfloor \Gamma^{\bar{v}}_{\bar{e}} \rfloor$, $\lceil \Gamma^{\bar{v}}_{\bar{e}} \rceil$, $\lfloor \Lambda^{\bar{v}}_{\bar{E}} \rfloor$, or $\lceil \Lambda^{\bar{v}}_{\bar{E}} \rceil$ depending on the specific branching rule applied). Furthermore, let $\boldsymbol{\xi} = (\xi_\psi \mid \psi \in \Upsilon)$ denote the vector of optimal dual

variables associated with the branching constraints. Let $\Delta(\Upsilon)$ denote the feasible region of the BDSP after incorporating the dual constraints associated with the active branching constraints. When CG is used to solve the BSP restricted to the route set $\mathcal{R}'$, the dual variables $\boldsymbol{\chi}$ are constructed as in (51), with an additional term accounting for the active branching constraints. Specifically, let M_ψ^v denote the largest coefficient of a route variable of type v in branching constraint ψ and let $\Upsilon^+ = \{\psi \in \Upsilon \mid \xi_\psi^* > 0\}$. We set

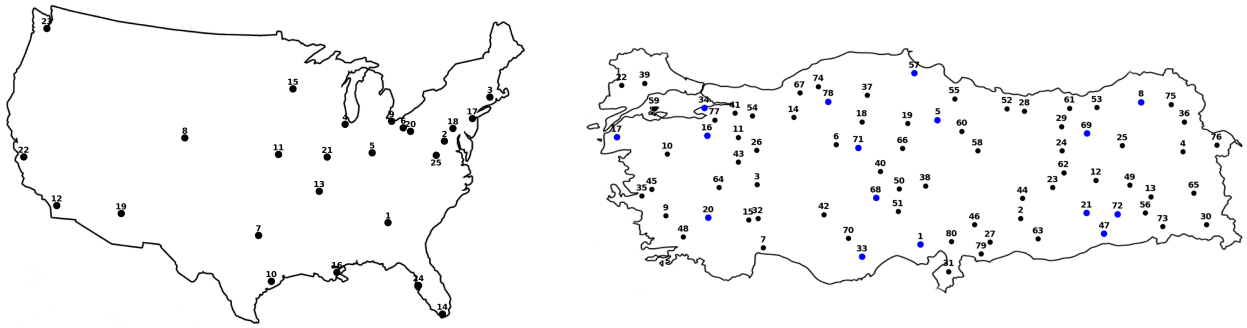
$$\chi_k^{v*} := \begin{cases} 0, & k \in \mathcal{H}', \\ -\max\left\{0, \alpha_v^* + \max_{k' \in \mathcal{H}} \beta_{k'}^{v*} - \min_{k' \in \mathcal{H}} \beta_{k'}^{v*} + LU_v\gamma - \kappa_v + \sum_{\psi \in \Upsilon^+} M_\psi^v \xi_\psi^*\right\}, & k \in \mathcal{H} \setminus \mathcal{H}', \end{cases} \quad \forall v \in \mathcal{V}. \tag{C.1}$$

Here, $M_\psi^v \le L$ for the first branching rule and $M_\psi^v = 1$ for the applicable aircraft type under the second and third rules. Only positive ξ_ψ^* can decrease the left-hand side of constraints (39); hence, the same argument as in Proposition 2 establishes that the constructed dual solution is feasible for the BDSP with the active branching constraints. Accordingly, the optimality cut in (48) is updated as follows:

$$\eta \ge \sum_{i \in \mathcal{N}} \sum_{k \in \mathcal{H}} \pi_{ik} \left(O_i x_{ik} - \sum_{j \in \mathcal{N}} w_{ij} x_{jk} \right) + \sum_{i \in \mathcal{N}} \sum_{k \in \mathcal{H}} O_i \lambda_{ik} x_{ik} + \sum_{v \in \mathcal{V}} |\mathcal{Q}_v| \alpha_v + \sum_{v \in \mathcal{V}} \sum_{k \in \mathcal{H}} |\mathcal{Q}_v| \chi_k^v y_k + \sum_{\psi \in \Upsilon} u_\psi \xi_\psi,$$
$$\forall (\boldsymbol{\pi}, \boldsymbol{\lambda}, \boldsymbol{\alpha}, \boldsymbol{\beta}, \boldsymbol{\rho}, \boldsymbol{\chi}, \boldsymbol{\xi}) \in \Delta(\Upsilon). \tag{C.2}$$

Appendix D: Details of Instance Generation and Parameter Settings

The locations of demand nodes and potential hub nodes for the CAB dataset and the TR dataset are shown in Figures D.1(a) and D.1(b), respectively. In these figures, black circles indicate demand nodes while the numbers represent the node indices in the corresponding dataset. In Figure D.1(b), we use blue circles to indicate the 16 potential hub nodes in the TR dataset.



(a) The 25 Demand Nodes in the CAB Dataset

(b) The 80 Demand Nodes and 16 Potential Hub Nodes in the TR dataset

Figure D.1 An Illustration of the CAB Dataset and the TR Dataset

Due to the high manufacturing costs and lengthy production cycles associated with new cargo aircraft, carriers primarily acquire them by purchasing mid-life retired passenger aircraft from commercial airlines and converting them into dedicated cargo aircraft (Zheng et al. 2024). Given this operational model, we consider all aircraft in our problem to be converted cargo aircraft. According to IATA (2016), we assume that the purchasing cost of a converted cargo aircraft is 15% of the price of a new passenger aircraft. Based on the new passenger aircraft prices reported in Chao and Hsu (2014), we estimate the purchasing costs of converted aircraft to be \$7.74 million, \$10.16 million, and

\$28.23 million for aircraft of type T1, T2, and T3, respectively, by applying the 15% factor. Moreover, we assume that carriers can put converted cargo aircraft into operation for an expected lifespan of approximately 20 years. Then, the daily fixed operating cost κ_v for a cargo aircraft of type $v \in \mathcal{V}$ can be calculated as the purchasing cost divided by $[20\,(\text{years}) \times 365\,(\text{days})]$. We consider the speed of 750 km/h for all types of aircraft. Let d_{ij} denote the distance of arc $(i,j) \in \mathcal{A}$. For a cargo aircraft of type $v \in \mathcal{V}$ traversing an arc $(k,m) \in \mathcal{A}_{\mathcal{H}}$, the transport cost $\mu^v_{km} = c^{var}_v \times d_{km}$, where c^{var}_v is the variable unit cost summarized in Table D.1. According to Boeing (2022), the numbers of standard-body, wide-body, and large wide-body cargo aircraft worldwide are in the approximate ratio of 1.5:1.3:1, corresponding to types T1, T2, and T3, respectively. Accordingly, we estimate the number of each type of cargo aircraft available for purchase based on their proportional quantities in our instances. The specific parameters of cargo aircraft are summarized in Table D.1.

Table D.1 Parameters of Cargo Aircraft Types in the Instances

Parameter and Description	Aircraft Type		
	T1	T2	T3
Capacity U_v (t)	15	28	54
Daily Fixed Cost κ_v (\$)	1060.27	1392.78	3867.12
Variable Cost c^{var}_v (\$/km)	3.88	6.38	7.77
Speed (km/h)	750	750	750

As cargo aircraft typically operate during late-night hours, such as from 11:00 PM to 8:00 AM (Yıldız and Savelsbergh 2022), we set the length of the planning horizon T to 9 hours. The travel time of cargo aircraft for each arc consists of two components: (i) the flying time calculated by dividing the distance of this arc by the aircraft's speed, subject to a minimum of 30 minutes, and (ii) an additional 40 minutes to include the time consumed while taxiing, securing takeoff and landing approvals (Yıldız et al. 2021). For each hub $k \in \mathcal{H}$, the turnaround time ω_k is set to 90 minutes.

We estimate a construction cost of \$1.5 billion for opening an air cargo hub. Assuming that the lifespan of a hub is 50 years, the fixed cost of opening a hub per day (i.e., f_k) is calculated by dividing this construction cost by $[50\,(\text{years}) \times 365\,(\text{days})]$. Following Ebery et al. (2000), the capacity S_k of each potential hub node $k \in \mathcal{H}$ is calculated as $S_k = \left(\frac{|\mathcal{N}|}{p} + \frac{3 d_{k i_0} O_k}{5 \max_{i \in \mathcal{N}} d_{i i_0} \max_{i \in \mathcal{N}} O_i} \right) O_k$, where node i_0 is the node that is closest to the center of mass of the network. The unit cost per weight for ground transportation is set to \$0.15 per ton-kilometer. Accordingly, for any arc between spoke $i \in \mathcal{N}$ and hub $k \in \mathcal{H}$, we have unit ground transportation cost $c_{ik} = 0.15 \times d_{ik}$ and $c_{ki} = 0.15 \times d_{ki}$. The unit weight penalty cost γ of delayed cargo is set to \$5,000 per ton, which satisfies the sufficient condition for the LBL inequality in Section 4.6.1 for all tested instances.

Appendix E: Implementation Details of the BPC Algorithm

This section details the application of the BPC algorithm to solve the ASHNDP. At each node of the branch-and-bound tree, the LP relaxation of model M2 is solved via CG. A critical distinction between the BPC algorithm and our solution approach lies in the construction of the state-space graph for the pricing problem. Although the pricing problem is solved using the same labeling algorithm as that used in our BD-B&B approach (see Online Appendix C.2 for details), the state-space graph in the BPC framework is built on the initial set of potential hub nodes $\mathcal{H}$. Specifically, the state-space graph is defined as $G_v = (\bar{\mathcal{H}}, \bar{\mathcal{A}}_H)$, where the node set is $\bar{\mathcal{H}} = \mathcal{H} \cup \{O, D\}$ with dummy source O and sink D. The arc set is given by $\bar{\mathcal{A}}_H = \mathcal{A}_O \cup \mathcal{A}_H \cup \mathcal{A}_D$, where $\mathcal{A}_O = \{(O,n) \mid n \in \mathcal{H}\}$ and $\mathcal{A}_D = \{(n,D) \mid n \in \mathcal{H}\}$.

Following Yıldız et al. (2021), we incorporate a class of cutting planes to further strengthen the LP relaxation of model M2. Specifically, whenever a node in the branch-and-bound tree yields an integer solution $(\bar{\boldsymbol{x}}, \bar{\boldsymbol{y}})$, we construct a set $D_{km}(\bar{\boldsymbol{x}}) = \{(i,j) \in \mathcal{N} \times \mathcal{N} \mid \bar{x}_{ik} + \bar{x}_{jm} - 1 > 0\}$ for each pair of distinct $k, m \in \mathcal{H}$. These cutting planes are formulated as follows:

$$\sum_{v \in \mathcal{V}} \sum_{r \in \mathcal{R}} B_{rkm} U_v \theta_r^v + \phi_{km} \geq \sum_{(i,j) \in D_{km}(\bar{\boldsymbol{x}})} w_{ij}(x_{ik} + x_{jm} - 1) \quad \forall k, m \in \mathcal{H} : k \neq m. \tag{E.1}$$

To enforce the integrality of the relaxed variables within the branch-and-bound framework, we implement a tailored branching strategy for the BPC algorithm. Specifically, we prioritize branching on the hub location variables $\boldsymbol{y}$, followed by the allocation variables $\boldsymbol{x}$. If a fractional variable exists in $\boldsymbol{y}$, we select the one closest to 0.5, denoted by $y_{\bar{k}}$, and split the current node into two child nodes by imposing branching constraints $y_{\bar{k}} = 0$ and $y_{\bar{k}} = 1$, respectively. If all variables in $\boldsymbol{y}$ are integral, we branch on the fractional variable $x_{\bar{i}\bar{k}}$ in $\boldsymbol{x}$ that is closest to 0.5, generating two child nodes with branching constraints $x_{\bar{i}\bar{k}} = 0$ and $x_{\bar{i}\bar{k}} = 1$, respectively. Once all $\boldsymbol{x}$ and $\boldsymbol{y}$ variables become integral, the hierarchical branching rule used in the BD-B&B approach (see Section 4.5 for details) is triggered to enforce the integrality of variables $\boldsymbol{\theta}$. When a new integer incumbent solution is identified, the upper bound is updated accordingly. The lower-bound updating rules are identical to those described for the BD-B&B approach in Section 4.

To enhance the performance of the BPC algorithm, we embed a heuristic at the root node. After solving the LP relaxation via CG, we reintroduce the integrality constraints of variables $\boldsymbol{x}$, $\boldsymbol{y}$, and $\boldsymbol{\theta}$ to the restricted master problem with the current set of cargo aircraft routes. This model is then directly solved with a computational time limit of 150 seconds. For instances where solving the root LP relaxation reaches the 3,600-second limit, we terminate CG and apply the heuristic to obtain a feasible integer solution. In such cases, we use the Lagrangian bound induced by the current RMP dual solution and the pricing problem as the local lower bound. This bound remains valid even when CG has not converged, and is therefore used to report a valid conservative optimality gap (Lübbecke and Desrosiers 2005).

Appendix F: The Sequential Decision Process for the ASHNDP

In the sequential decision process, we solve two MILP models sequentially. The first model, denoted by S1, addresses the hub location component of the ASHNDP. After solving S1, we obtain the hub location and allocation decisions $(\boldsymbol{x}^*, \boldsymbol{y}^*)$. Fixing these decisions, we then solve the second model, denoted by S2, which addresses the service network design component of the ASHNDP. The S1 model is formulated as follows:

$$[\textbf{S1}] \min \sum_{k \in \mathcal{H}} f_k y_k + \sum_{i \in \mathcal{N}} \sum_{k \in \mathcal{H}} c_{ik} O_i x_{ik} + \sum_{i \in \mathcal{N}} \sum_{k \in \mathcal{H}} c_{ki} D_i x_{ik} \tag{F.1}$$
$$\text{s.t. } (2)\text{–}(8), (17)\text{–}(18), (20).$$

Using the solution $(\boldsymbol{x}^*, \boldsymbol{y}^*)$ from S1, the following model S2 is solved:

$$[\textbf{S2}] \min \sum_{q \in \mathcal{Q}} \kappa_q \delta_q + \sum_{q \in \mathcal{Q}} \sum_{l \in [L]} \sum_{k \in \mathcal{H}} \sum_{m \in \mathcal{H}: m \neq k} \mu_{km}^q z_{km}^{ql} + \sum_{k \in \mathcal{H}} \sum_{m \in \mathcal{H}: m \neq k} \gamma \phi_{km} \tag{F.2}$$
$$\text{s.t. } (9)\text{–}(13), (16), (19), (20), (21),$$
$$\sum_{m \in \mathcal{H}: m \neq k} g_{ikm} + \sum_{j \in \mathcal{N}} w_{ij} x_{jk}^* = \sum_{m \in \mathcal{H}: m \neq k} g_{imk} + O_i x_{ik}^* \quad \forall i \in \mathcal{N}, k \in \mathcal{H}, \tag{F.3}$$
$$\sum_{m \in \mathcal{H}: m \neq k} g_{ikm} \leq O_i x_{ik}^* \quad \forall i \in \mathcal{N}, k \in \mathcal{H}, \tag{F.4}$$
$$z_{km}^{ql} \leq y_k^* \quad \forall k, m \in \mathcal{H} : k \neq m, q \in \mathcal{Q}, l \in [L], \tag{F.5}$$
$$z_{km}^{ql} \leq y_m^* \quad \forall k, m \in \mathcal{H} : k \neq m, q \in \mathcal{Q}, l \in [L]. \tag{F.6}$$

Appendix G: Additional Computational Results

In this section, we provide additional computational results related to Sections 5.4, 5.5, and 5.6.

G.1. Results of the BD-B&B Approach with and without HEU and BBC on the TR Dataset

Table G.1 presents the results of the comparison of the BD-B&B approach with and without HEU and BBC strategies on the TR instances. For instances TR-1 to TR-5, the BD-B&B approaches with and without HEU exhibit similar computational performance, solving all five instances to optimality with average CPU times of 331 and 335 seconds, respectively. However, without HEU, the BD-B&B approach fails to find a feasible solution for instances TR-6 to TR-20. For instances TR-1 to TR-5, BBC reduces the average CPU time from 1,393 to 331 seconds. For instances TR-6 to TR-20, BBC enables the algorithm to solve more BMPs within the time limit and reduces the average optimality gap by 0.03%–0.36%.

Table G.1 Comparison of the BD-B&B Approach with and without HEU and BBC Strategies on the TR Dataset

Instance	Parameters					No HEU				No BBC				BD-B&B			
	p	W	T1	T2	T3	#BMP	Obj	Gap	CPU	#BMP	Obj	Gap	CPU	#BMP	Obj	Gap	CPU
TR-1	2	2000	8	7	5	15	471000.75	0.00	264	31	471450.64	0.10	3251	15	471450.64	0.10	299
TR-2	2	2500	10	8	7	21	547157.72	0.00	460	27	547698.21	0.08	1550	21	547698.21	0.10	504
TR-3	2	3000	11	10	8	25	623519.43	0.00	474	19	623945.77	0.08	856	19	623945.77	0.10	367
TR-4	2	3500	13	11	9	9	700384.53	0.00	119	37	701056.94	0.08	711	9	701056.94	0.10	130
TR-5	2	4000	15	13	10	31	776704.02	0.00	360	37	777427.40	0.08	598	31	777427.40	0.09	354
Average	2	3000	11.40	9.80	7.80	20	623753.29	0.00	335	30	624315.79	0.08	1393	19	624315.79	0.10	331
TR-6	3	2000	8	7	5	14	–	100.00	3600	8	561505.85	1.67	3600	14	561295.30	1.56	3600
TR-7	3	2500	10	8	7	20	–	100.00	3600	10	637379.77	1.39	3600	18	637379.77	1.28	3600
TR-8	3	3000	11	10	8	34	–	100.00	3600	8	713386.75	1.18	3600	30	713256.13	0.97	3600
TR-9	3	3500	13	11	9	52	–	100.00	3600	10	790565.26	1.16	3600	52	786355.97	0.39	3600
TR-10	3	4000	15	13	10	50	–	100.00	3600	10	867710.00	1.14	3600	50	864611.49	0.53	3600
Average	3	3000	11.40	9.80	7.80	34	–	100.00	3600	9	714109.53	1.31	3600	33	712579.73	0.95	3600
TR-11	4	2000	8	7	5	12	–	100.00	3600	8	649599.37	2.34	3600	12	649072.07	2.18	3600
TR-12	4	2500	10	8	7	12	–	100.00	3600	8	725526.76	2.02	3600	12	725526.76	1.92	3600
TR-13	4	3000	11	10	8	12	–	100.00	3600	6	801454.15	1.76	3600	12	801454.15	1.66	3600
TR-14	4	3500	13	11	9	12	–	100.00	3600	8	878398.10	1.66	3600	12	878190.18	1.53	3600
TR-15	4	4000	15	13	10	14	–	100.00	3600	8	954325.49	1.46	3600	14	954072.28	1.33	3600
Average	4	3000	11.40	9.80	7.80	12	–	100.00	3600	8	801860.77	1.85	3600	12	801663.09	1.72	3600
TR-16	5	2000	8	7	5	10	–	100.00	3600	6	737606.87	2.82	3600	10	736513.34	2.62	3600
TR-17	5	2500	10	8	7	10	–	100.00	3600	6	810254.74	2.08	3600	10	812375.28	2.28	3600
TR-18	5	3000	11	10	8	10	–	100.00	3600	6	887176.95	1.94	3600	12	887176.95	1.86	3600
TR-19	5	3500	13	11	9	10	–	100.00	3600	6	964055.45	1.83	3600	10	964055.45	1.76	3600
TR-20	5	4000	15	13	10	14	–	100.00	3600	6	1042063.84	1.83	3600	14	1043124.11	1.84	3600
Average	5	3000	11.40	9.80	7.80	11	–	100.00	3600	6	888231.57	2.10	3600	11	888649.03	2.07	3600

Note. We use "–" to indicate that no feasible solution was found within the time limit.

G.2. Detailed Results on the Effects of Key Problem Parameters

This subsection examines how the number of selected hubs p, the cardinality $|\mathcal{H}|$ of the set of potential hub nodes, and the numbers $|\mathcal{Q}_v|$ of cargo aircraft of each type $v \in \mathcal{V}$ available for purchase affect the gap between M2 and $\overline{\text{M2}}$ and the computational performance of the BD-B&B approach. We generate small-scale instances using the first ten cities in the CAB dataset and the corresponding distance and demand data and set $|\mathcal{N}| = 10$ and $W = 400$. Both M2 and $\overline{\text{M2}}$ can be solved to optimality for these instances. The baseline setting is $|\mathcal{H}| = 10$, $p = 3$, and $(|\mathcal{Q}_{\text{T1}}|, |\mathcal{Q}_{\text{T2}}|, |\mathcal{Q}_{\text{T3}}|) = (2, 2, 1)$. We vary one of these three parameters at a time, fixing the other two at their baseline values and keeping all remaining instance parameters unchanged. Let $\mathscr{Z}(\text{M2})$ and $\mathscr{Z}(\overline{\text{M2}})$ denote the optimal objective values of the two models, respectively, and calculate their gap as $[\mathscr{Z}(\text{M2}) - \mathscr{Z}(\overline{\text{M2}})]/\mathscr{Z}(\text{M2}) \times 100\%$. Table G.2 reports the results.

As p increases from 2 to 4, the gap between M2 and $\overline{\text{M2}}$, the number of explored B&B nodes, and CPU time all increase, showing that the instances become markedly more difficult to solve. A larger p expands the solution space

Table G.2 Computational Results under Different Parameter Settings

Parameter	Value	$\mathscr{Z}(\overline{\text{M2}})$	$\mathscr{Z}(\text{M2})$	Gap (%)	Nodes	CPU (s)
p	2	217450.05	219515.17	0.94	11	1
	3	299599.86	308131.18	2.77	1561	75
	4	383114.21	395320.28	3.09	10533	1632
$\lvert\mathcal{H}\rvert$	6	303911.15	312426.95	2.73	405	13
	8	301929.46	310609.58	2.79	1165	49
	10	299599.86	308131.18	2.77	1561	75
$(\lvert\mathcal{Q}_{\text{T1}}\rvert, \lvert\mathcal{Q}_{\text{T2}}\rvert, \lvert\mathcal{Q}_{\text{T3}}\rvert)$	$(1,1,1)$	299599.86	309912.54	3.33	697	81
	$(2,2,1)$	299599.86	308131.18	2.77	1561	75
	$(3,3,2)$	298530.79	307265.81	2.84	897	47

Note. Column *Nodes* reports the number of nodes explored in the main B&B tree.

of the hub-location and allocation decisions and enlarges the state-space graph used in the pricing problem, with the number of potential aircraft routes growing on the order of $O(p^L)$. These structural changes make the resulting instances more difficult for the BD-B&B approach to solve. As $|\mathcal{H}|$ increases from 6 to 8 and 10, the gap remains nearly stable at 2.73%, 2.79%, and 2.77%, respectively, whereas the number of explored nodes and CPU time increase monotonically. Thus, increasing $|\mathcal{H}|$ makes the instances more difficult to solve even though the gap between M2 and $\overline{\text{M2}}$ changes little. Regarding the aircraft-availability settings, under $(1,1,1)$, $(2,2,1)$, and $(3,3,2)$, the gaps are 3.33%, 2.77%, and 2.84%, respectively. Although the gap and the number of explored nodes vary nonmonotonically as more aircraft become available, CPU time decreases from 81 to 75 and 47 seconds.

Overall, a smaller gap between M2 and $\overline{\text{M2}}$ provides a tighter relaxation and facilitates bound-based fathoming, but the gap and B&B tree size do not exhibit a consistent monotonic relationship across the parameter settings considered. This observation is consistent with Shah et al. (2026), who show that B&B tree size need not be monotonic with respect to relaxation strength because changes in the relaxation solutions may alter subsequent branching decisions. CPU time depends on both the number of explored nodes and the time required by the BD algorithm to solve $\overline{\text{M2}}$ with the branching constraints imposed at each node. The results further show that larger values of p and $|\mathcal{H}|$ increase computational difficulty, whereas greater aircraft availability tends to reduce CPU time in the instances considered.

G.3. Results of the Tests for the Value of Integration on the TR Dataset

Table G.3 compares the results obtained from solving the TR instances using the BD-B&B approach and the sequential decision process. As shown in Table G.3, the solutions produced by the BD-B&B approach require, on average, 83.33%–89.09% fewer cargo aircraft. Moreover, this approach reduces the total operational costs of air service hub networks by an average of 38.96%–78.94% for instances with $\sigma \in \{0.5, 1.0\}$, and by 14.58%–14.71% for instances with $\sigma \in \{1.5, 2.0\}$, compared with the sequential decision process.

G.4. Hub Location and Spoke Allocation under Different Planning Horizons

In this section, we examine the changes in the locations of hubs and allocation of spokes to hubs for instances under different planning horizons T. The changes in the locations of hubs and allocation of spokes to hubs are presented in Figure G.1, with only the case of $p = 3$ presented herein. For instances with $T \leq 11$, the selected hubs and their spoke allocations are relatively concentrated; in particular, the hub-location and spoke-allocation decisions are identical for $T \in \{7, 9, 11\}$. In contrast, for the instance with $T = 13$, the selected hubs are more geographically dispersed and the spokes are allocated more evenly among them. This is because a shorter T restricts the number of flights that each cargo aircraft can operate. When cargo aircraft resources are limited, assigning more spokes to a single hub enables more cargo to be routed through a spoke-hub-spoke pattern (i.e., passing through only one hub). As this pattern relies solely on ground transportation, it helps reduce cargo delays resulting from insufficient aircraft availability.

Table G.3 Value of Integration on the TR Dataset

σ	p	Sequential Decision Process			BD-B&B			IP Gap
		Obj	Hubs	#Air	Obj	Hubs	#Air	
0.5	2	2712280.00	[34, 58]	20	623945.77	[6, 18]	1	77.00
0.5	3	3020833.88	[6, 21, 34]	20	712403.96	[6, 18, 69]	2	76.42
0.5	4	4188565.07	[6, 21, 34, 35]	20	801454.15	[6, 18, 69, 79]	4	80.87
0.5	5	4782504.08	[6, 21, 34, 35, 58]	20	886116.67	[6, 18, 69, 70, 79]	4	81.47
Average		3676045.76	–	20.00	755980.14	–	2.75	78.94
1.0	2	821938.67	[34, 58]	25	623945.77	[6, 18]	1	24.09
1.0	3	879701.12	[6, 21, 34]	27	709230.33	[6, 18, 70]	2	19.38
1.0	4	1439093.56	[6, 21, 34, 35]	29	801454.15	[6, 18, 69, 79]	4	44.31
1.0	5	2775806.85	[6, 21, 34, 35, 58]	29	887176.95	[6, 18, 69, 70, 79]	5	68.04
Average		1479135.05	–	27.50	755451.80	–	3.00	38.96
1.5	2	762354.79	[34, 58]	15	624949.84	[6, 70]	1	18.02
1.5	3	826112.40	[6, 21, 34]	18	713256.13	[6, 18, 48]	2	13.66
1.5	4	925111.52	[6, 21, 34, 35]	23	801454.15	[6, 18, 69, 79]	4	13.37
1.5	5	1030198.68	[6, 21, 34, 35, 58]	36	888237.22	[6, 18, 69, 70, 79]	6	13.78
Average		885944.35	–	23.00	756974.34	–	3.25	14.71
2.0	2	762354.79	[34, 58]	15	624949.84	[6, 70]	1	18.02
2.0	3	825271.53	[6, 21, 34]	17	713464.23	[6, 18, 69]	3	13.55
2.0	4	914749.94	[6, 21, 34, 35]	21	801454.15	[6, 18, 69, 79]	4	12.39
2.0	5	1036878.60	[6, 21, 34, 35, 58]	31	888237.22	[6, 18, 69, 70, 79]	6	14.34
Average		884813.72	–	21.00	757026.36	–	3.50	14.58

Note. We use "–" to denote that the average value is not defined for the locations of hubs.

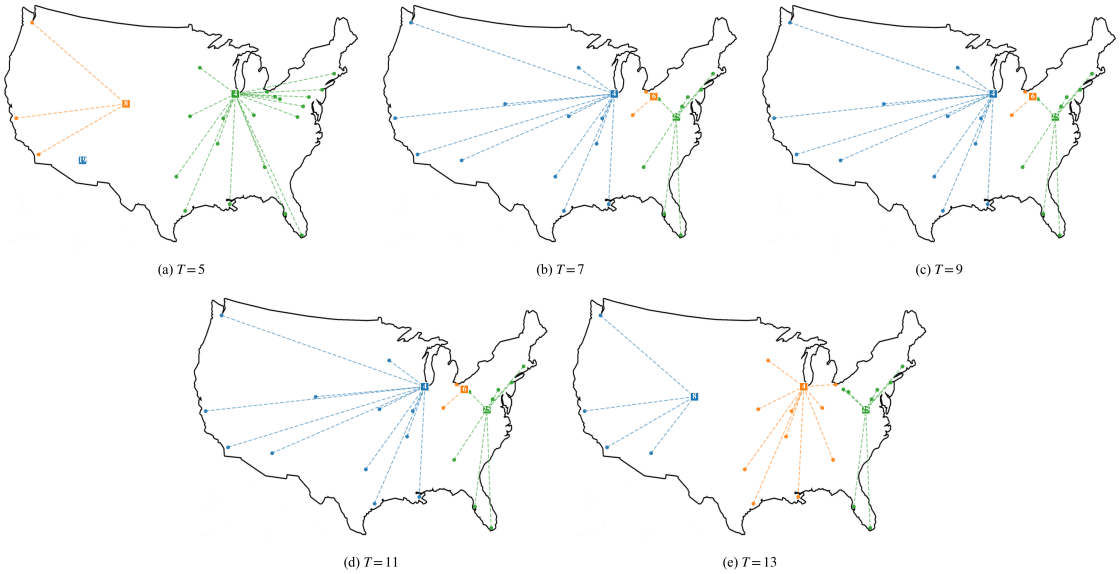


Figure G.1 Hub Location Solutions under Different Planning Horizons

References

Benders J (1962) Partitioning procedures for solving mixed-variables programming problems. *Numerische Mathematik* 4(1):238–252.

Boeing (2022) World air cargo forecast 2022–2041. Technical report, Boeing.

Chao CC, Hsu CW (2014) Cost analysis of air cargo transport and effects of fluctuations in fuel price. *Journal of Air Transport Management* 35:51–56.

Desaulniers G, Gschwind T, Irnich S (2020) Variable fixing for two-arc sequences in branch-price-and-cut algorithms on path-based models. *Transportation Science* 54(5):1170–1188.

Ebery J, Krishnamoorthy M, Ernst A, Boland N (2000) The capacitated multiple allocation hub location problem: Formulations and algorithms. *European Journal of Operational Research* 120(3):614–631.

IATA (2016) Airline disclosure guide aircraft acquisition cost and depreciation. Accessed September 19, 2025, https://www.iata.org/contentassets/4a4b100c43794398baf73dcea6b5ad42/airline-disclosure-guide-aircraft-acquisition.pdf.

Lübbecke ME, Desrosiers J (2005) Selected topics in column generation. *Operations Research* 53(6):1007–1023.

Shah P, Dey SS, Molinaro M (2026) Non-monotonicity of branching rules with respect to linear relaxations. *INFORMS Journal on Computing* 38(1):53–66.

Yıldız B, Savelsbergh M (2022) Optimizing package express operations in China. *European Journal of Operational Research* 300(1):320–335.

Yıldız B, Yaman H, Karaşan OE (2021) Hub location, routing, and route dimensioning: Strategic and tactical intermodal transportation hub network design. *Transportation Science* 55(6):1351–1369.

Zheng S, Wang K, Jiang C (2024) Converting passenger aircraft into cargo planes under volatile market demand. *Transportation Research Part A: Policy and Practice* 181:104013.